Received 00th January 20xx,
Accepted 00th January 20xx

DOI: xxxxx/x0xx00000x

Synthesis of graphene nanoribbons with defined mixed edge-site sequence by surface assisted polymerization of (1,6)-dibromopyrene on Ag(110)

Marco Smerieri[a], Igor Píš[b,c,+], Lara Ferrighi[d], Silvia Nappini[c], Angelique Lusuan[a,e], Cristiana Di Valentin[d], Luca Vaghi[d], Antonio Papagni[d], Mattia Cattelan[f,§], Stefano Agnoli[f], Elena Magnano[c,g], Federica Bondino[c] and Letizia Savio[a,+]

By a combination of scanning tunneling microscopy, X-ray spectroscopic techniques and density functional theory calculations, we prove the formation of extended patterns of parallel, graphene nanoribbons with alternated zig-zag and armchair edges and selected width by surface assisted Ullmann coupling polymerization and dehydrogenation of 1,6-dibromopyrene ($C_{16}H_8Br_2$) . Besides the relevance of these nanostructures for their possible application in nanodevices, we demonstrate the peculiarity of halogenated pyrene derivatives for the formation of nanoribbons, in particular on Ag(110). These results open the possibility of tuning the shape and dimension of nanoribbons (and hence the correlated electronic properties) by choosing suitably tailored or on-purpose designed molecular precursors.

1. Introduction

Graphene, a single layer of hexagonally packed π-conjugated C atoms, has attracted a large attention in the last years due to its excellent electronic, mechanical and thermal properties[1, 2] and, recently, has been the subject of extensive investigation. However, its intrinsic zero-energy gap reduces its impact for applications in nanodevices (e.g. for the building of graphene-based FETs), for which a semiconducting behaviour and the presence of a well-defined band gap is essential.[3] Therefore, nowadays the interest has shifted towards graphene-based nanostructures, and in particular towards the so-called graphene nanoribbons (GNRs). If narrower than 10 nm, GNRs owe semiconducting properties due to electron confinement in one dimension and edge structure effects.[4-6] It has also been demonstrated that, when grown on sidewall facets of SiC, GNRs present very good ballistic transport, comparable with the one of metallic carbon nanotubes.[7, 8] These nanostructures can be produced by a top-down approach, using chemical[9], sonochemical[4] and lithographic[10] methods as well as unzipping carbon nanotubes.[11, 12] However, such approach leads to

[a] IMEM-CNR, UOS Genova, Via Dodecaneso 33, 16146 Genova, IT
[b] Elettra-Sincrotrone Trieste S.C.p.A., S.S. 14 km 163.5, 34149 Basovizza (TS), IT
[c] IOM-CNR, Laboratorio TASC, S.S. 14 km 163.5, 34149 Basovizza (TS), IT
[d] Dipartimento di Scienza dei Materiali, Università di Milano-Bicocca, Via R. Cozzi 55, 20125 Milano, IT
[e] Dipartimento di Fisica, Università di Genova, Via Dodecaneso 33, 16146 Genova, IT
[f] Department of Chemical Science, University of Padova. Via F. Marzolo 1, 35131 Padova, IT
[g] Department of Physics, University of Johannesburg, PO Box 524, Auckland Park, 2006, Johannesburg, South Africa
+ Corresponding authors: letizia.savio@imem.cnr.it; igor.pis@elettra.eu
§ Present address: School of Chemistry, University of Bristol, Bristol BS8 1TS, United Kingdom
† Electronic Supplementary Information (ESI) available: additional experimental data (temperature programmed XPS, NEXAFS, STM) and simulated structures. See DOI: xxxx/x0xx00000x

nanostructures with rough edges and, consequently, to a reduced charge carrier mobility. A bottom-up approach, which exploits the surface-catalysed covalent coupling of suitable halogenated precursors, is a more reliable method for the production of GNR with well-defined size and shape.

It is now well established that the polymerization process at the base of the bottom-up production of graphene nanostructures on noble metals occurs in two steps. The former is the de-halogenation process, which often involves the formation of an organometallic intermediate with metal atoms extracted from the surface, followed by a surface-catalysed C–C bond formation. This reaction, known as Ullman coupling, has been deeply investigated and exploited in several surface-mediated polymerization processes.[13-17] The latter consists of a thermally induced dehydrogenation of these surface species with the formation of further C–C covalent bonds. In the last years, several experimental and theoretical works have characterized both the graphene-based nanostructures and the chemical path leading from the molecular precursors to the final products. Both organometallic intermediates and final products are strongly dependent on the nature of the initial halogenated precursor as well as on the chemical nature and atomic structure of the substrate. Cai et al. showed that straight armchair GNRs with only 7 rows of carbon atoms (usually indicated as N=7) can be fabricated on Ag(111)[18] single crystals starting from the 10,10'-dibromo-9,9'-bianthryl (DBBA) precursor, while chevron-type GNRs with alternating widths of N=6 and N=9 are obtained using 6,11-dibromo-1,2,3,4-tetraphenyltriphenylene precursor monomers on the same substrate. The former molecule is one of the most commonly studied precursors and it has been the subject of further investigations. The nature of the substrate has a determining role in the formation of GNRs, as evidenced by comparing the results obtained on Au(111) and Cu(111).[19] On Au(111) the GNR growth mechanism is catalysed by the surface, which favours the precursor de-halogenation followed by polymerization and dehydrogenation; the latter processes are thermally activated by annealing steps at 200 °C and 400 °C, respectively, leading to the formation of graphene-like ribbon assemblies[18]. On the more reactive Cu(111) surface, de-halogenation occurs at room temperature (RT) and the formation of GNRs is observed already at 250 °C. Also the surface atomic structure was proved to be relevant. On both Au(111) and Au(110) a reaction path is active for deposition of DBBA at RT; on the latter surface, however, an alternative path opens up at high temperature. Furthermore, long-range ordering of GNRs can be achieved on the Au(788) vicinal surface, since the terrace anisotropy favours the synthesis of parallel structures[20, 21]. When depositing a DBBA layer on copper, the same thermal treatment leads to GNR formation on Cu(111), while on Cu(110) the Ullman coupling reaction is blocked by the strong anisotropy of the surface and quasi-zero dimension flat nanographene units form[22].

The nature of the molecule is another crucial ingredient to determine the geometry of graphene nanostructures. For nanoribbons in particular, the attention is focussed on the edge morphology; species with armchair[18], ziz-zag[23], cove[24] or chiral[25-27] edges have been identified so far and there is evidence of specific electronic states at the different edge sites. While several aromatic molecules have been demonstrated to self-assemble in well-organized organo-metallic compounds[28-30], only in a few cases complete dehydrogenation and C–C covalent bond formation are reported[18, 31, 32]. Some of us have recently investigated the on-surface polymerization of 5,11-dibromotetracene on Cu(110), Ag(110) and Au(111)[33-35], finding that graphene nanopatches are the ultimate product of the annealing process on the most reactive copper surface. On Ag(110) and Au(111), on the contrary, significant desorption occurs above 300 °C, before the onset of dehydrogenation and intermolecular C–C covalent coupling. The debrominated tetracene monomers are strongly adsorbed in the troughs between the high-density substrate atomic rows. Apparently, the preferential molecular orientation along the <1-10> direction, driven by the substrate anisotropy, and the formation of C–Ag bonds reduce the mobility required to achieve the rearrangement of monomers necessary for covalent polymerization of halogenated dibromotetracene. Nonetheless, once a more appropriate precursor molecule can be found, Ag is an interesting substrate for the bottom-up synthesis of GNRs due to its intermediate reactivity between Cu and Au.

Here we report on a combined experimental and theoretical investigation of the surface-catalysed polymerization reaction of 1,6-dibromopyrene (DBP) on Ag(110). The brominated pyrene derivative was chosen as a prototypical planar polycyclic hydrocarbon molecule with similar molecular weight but different shape with respect to the rod-like dibromotetracene. We show the self-assembled structures generated upon annealing the DBP multilayer to 150 °C and discuss their subsequent, thermally induced dehydrogenation. As final product, we observe the formation of C–conjugated polymers with alternated zig-zag and armchair edge sites, the length and order of which can be tuned by acting both on the annealing process and on the initial DBP coverage. These GNRs are monodispersed in width and significantly narrower than those obtained from the much more common DBBA precursor. As a direct consequence of the nature of the chosen precursor molecules, also the reaction path leading to surface assisted polymerization of DBP is quite different from the case of DBBA.

Besides being relevant for the possible application in nanodevices[3], our result shows the peculiarity of pyrene derivatives for the formation of nanoribbons on coinage metals and provides an excellent example of the possibility to tune the desired geometrical and electronic properties of the GNRs through the choice of an appropriate, on-purpose designed precursor.

2. Methods

Synthesis of 1,6-dibromopyrene. 1,6-dibromopyrene (see inset in Figure 1A for the molecular structure) is commercially available, but it was synthesized via direct bromination of pyrene following the procedure reported in Ref.[36]. Slow addition of bromine (1 ml, 19.5 mmol) in $CHCl_3$ (50 ml) to a solution of pyrene (2g, 9.9 mmol) in $CHCl_3$ (50 ml) produced a 1,6 and 1,8 dibromo isomeric mixture from which pure 1,6-dibromopyrene is obtained by fractional crystallization from xylene (0.97 g, 27%). Physical and spectroscopic data are in line with a 1,6-dibromopyrene commercial sample.

Experimental characterization. Experiments were performed in different apparatuses. In all cases the Ag (110) surface was cleaned by cycles of sputtering with noble gas ions (either Ne or Ar) followed by prolonged annealing to T=427 °C or T=600 °C for spectroscopy and microscopy experiments, respectively. Surface cleanliness and order were checked by low-energy electron diffraction (LEED) and by low temperature scanning tunneling microscopy (LT-STM) or X-ray photoelectron spectroscopy (XPS).

DBP was deposited on Ag(110) at RT and in a background pressure always lower than 2.0 10^{-9} mbar, by using a Ta crucible resistively heated to 100 °C. Then the system was step-annealed up to T= 475 °C in order to monitor the formation and thermal evolution of self-assembled organometallic species. The DBP coverage (Θ) is evaluated *a posteriori* from the intensity of the photoemission signal or by inspection of STM images. One monolayer coverage is defined as the amount of DBP left on the fully-covered surface after heating a DBP multilayer to 150 °C, which corresponds to (1.0 ± 0.1) DBP molecules/nm^2 according to statistical analysis of STM images.

STM experiments were carried out in Genova, in an ultra-high vacuum (UHV) apparatus consisting of a main chamber, hosting a low-temperature STM (Createc manufacturer), and of a preparation chamber equipped with a homemade evaporator for deposition of organic molecules and with all typical vacuum facilities for sample cleaning and residual gas analysis. STM images were recorded with the microscope cooled at liquid nitrogen temperature, using a Pt/Ir tip cut in air under strain and then reshaped by controlled crashes into the surface, so that tunneling occurs effectively through an Ag tip. The images were acquired in constant current mode, with typical tunneling currents of 0.15 nA and a bias voltage -250 mV<V<500 mV applied to the sample. Surface orientation and image dimensions were determined from atomically resolved measurements of the clean Ag(110) surface (see inset of Figure 1A); similarly, heights were calibrated on monatomic Ag steps. STM analysis was performed with the help of WSxM software[37].

High-resolution synchrotron-excited X-ray photoemission spectroscopy (XPS) measurements were carried out at the BACH beamline at the Elettra synchrotron (Trieste, Italy), in an UHV chamber with the base pressure lower than 1×10^{-9} mbar and equipped with a hemispherical electron energy analyzer (VG Scienta model R3000). The photoemission spectra were recorded at the emission angle of 60° from the surface normal. Photon energies hν=277 eV and 379 eV were employed to excite Br 3d and C 1s core levels. A total energy resolution of 0.15 eV for both photon energies was calculated from the width of the Fermi edge. All photemission binding energies (E_b) are referenced to the substrate Fermi level. The Br 3d spectra were decomposed into spectral components using Voigt doublet line shapes and C 1s spectra were fitted with Doniach–Šunjić line shapes convoluted with Gaussian profile, including Shirley type background.

Temperature programmed reaction (TPR) experiments were carried out in Padova, using a custom designed UHV system operating at a base pressure of 1x10^{-10} mbar and equipped with a HIDEN quadrupole mass spectrometer (QMS). The Ag(110) sample was fixed to the manipulator by a Ta frame using conductive ceramic glue and a K-type thermocouple was clipped on the back of the sample. T was varied between -150°C and 630°C. TPR spectra were acquired with a heating rate β=2.5 °C/sec. To record the desorption spectra, the 6 mm diameter orifice of the QMS was brought close to the sample surface (1 mm) in order to reduce spurious signals from the Ta filaments and to maximize the signal.

Theoretical methods. The adsorption of DBP molecules on a Ag(110) surface was modeled by using the recent Van der Waals density functional vdW-DF2^{C09x}, which was proven to give accurate description of the adsorption energies and distances of graphene on metal surfaces[38] and has also been successfully applied to describe self-assembly of brominated tetracene (DBT) on different metal surfaces[33-35]. Ag (110) 4×7 and 3×7 supercell models were used, with a vacuum layer of about 20 Å perpendicular to the surface to avoid interactions between the images. The Ag surface was modeled by a five-layer slab, where the three top layers and the adsorbate were allowed to fully relax, and the two bottom layers were kept fixed at the Ag optimized lattice parameter (4.10 Å with vdW-DF2^{C09x}). The Perdew-Burke-Ernzerhof (PBE) standard ultrasoft pseudopotentials, as implemented in the plane-wave based Quantum Espresso package,[39] were used with energy cutoff of 30 and 240 Ryd (for kinetic-energy and charge-density grids, respectively). The calculations were performed with a Gamma point sampling of the Brillouin zone, but a few check tests with a 2×2×1 grid were carried out, showing a negligible influence on the binding energies, as already observed in the literature for similar cases[33]. The STM image simulations were obtained within the Tersoff–Hamann approximation,[40] in which the tunneling current is considered to be proportional to the integrated local density of the states

in a given energy window, determined by the bias voltage, as applied in the corresponding experiments.

3. Results and Discussion

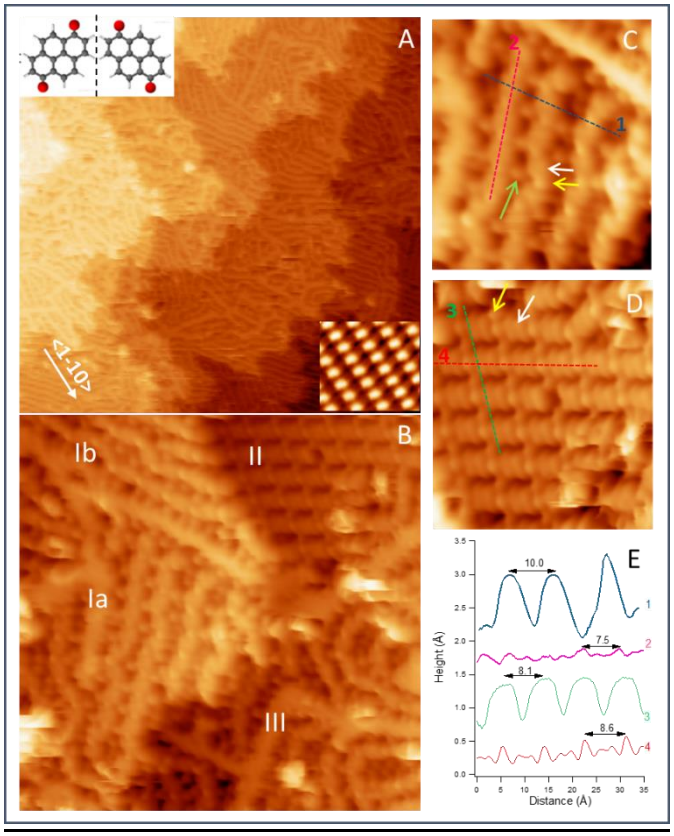

Figure 1. *STM images of the Ag(110) surface after deposition of DBP at RT (Θ>1 ML) and annealing to 150 °C. A) Overview of the surface, fully covered by DBP structures. (Image size: 45.3x45.3 nm², V=-50 mV, I= 10 nA). The <1-10> direction, deduced from atomically resolved images of the clean Ag(110) (bottom-right inset, 1.8x1.6 nm²) is marked. The structure of the (1,6)-dibromopyrene molecule is shown in the top-left corner. Both the enantiomeric configurations arising upon adsorption are reported. B) Close-up of the surface showing the co-existence of domains with different DBP structures. (Image size: 12.6x12.6 nm², V=-150 mV, I= 10 nA). C-D) High resolution images of structures Ia and II, respectively (Image size: 5.2x6.0 nm², V=150 mV, I= 18 nA). White arrows indicate the features corresponding to the DBP unit, the yellow and green ones the additional bright protrusions. E) Line profiles cut along the dashed lines marked in panels C and D and showing the typical periodicities of the DBP overlayer across (1 and 3) and along (2 and 4) the adsorbate chains.*

When depositing a DBP multilayer on Ag(110) at RT, the strong interaction between the STM tip and the weakly bound molecules of the second layer allows to image only a disordered and poorly resolved structure (not shown). As evident from Figure 1AB, annealing to 150° C causes desorption of the multilayer and the appearance of different molecular networks covering the entire Ag(110) surface. Domains marked as Ia and Ib have a similar molecular arrangement but different orientation, while domains denoted as II clearly present a diverse geometry. Finally, pattern III consists of molecules arranged in a much more disordered way and it covers areas in-between self-assembled islands. From a careful analysis of high resolution STM images as those reported in panels C and D, we understand that in structure I, which is the most abundant on the surface, molecules are arranged in rows extending preferentially -25° or +45° off the <1-10> direction and separated by ~10 Å on average (see line scan 1). Each row appears as a sequence of larger protrusions (marked by the white arrow) alternated with smaller and slightly brighter spots (yellow arrow). Approximately in correspondence of these spots, additional features of the same circular shape are present in-between the rows (green arrow). The periodicity of ~7.5 Å along the rows (see line scan 2) is compatible with the molecular dimensions, thus suggesting that each large protrusion corresponds to one DBP unit. In structure II, molecules are arranged in rows extending preferentially -53° and +21° off the <1-10> direction and separated by 8.1 Å on average. The DBP units (white arrow) appear as planar four-lobe structures, thus providing a sub-molecular resolution of the single benzene rings forming the molecular body. These features are well reproduced in the optimized geometry of isolated monomers calculated by density functional theory (DFT) and in the corresponding simulated STM images (see Figure S4 in the ESI). The flat-lying geometry of the deposited molecules is further confirmed by near-edge X-ray absorption fine structure spectroscopy (Figure S2 in ESI). Also in structure II, DBP units alternate in the row with couples of slightly brighter features (yellow arrow), showing an overall periodicity within the chain of~ 8.6 Å.

DBP is a planar molecule presenting two enantiofaces (two sides of the molecular plane), thus its adsorption on the metal surface creates two enantiomeric metal-DBP systems,[41] (shown in the top-left inset of Figure 1A), expected to be formed with equal probability. Close inspection of structure II evidences that all the DBP units have exactly the same orientation with respect to the surface directions and that the relative position of the four benzene rings within the molecule is the same. This is indicative of a preferential selection of one metal-DBP enantioface upon adsorption at the surface. On the contrary, many of the molecular rows in structure I show a slight (often not perfectly regular) zig-zag shape, which is compatible with an alternate or even random assembly of the two metal-DBP enantiomers (thus with an achiral structure).

The round protrusions in both structures I and II are difficult to identify due to the lack of chemical sensitivity of STM. They can be either Br atoms, Ag atoms or Br-Ag complexes. Their nature will be discussed therefore in light of the X-ray photoemission spectra obtained for a 1.2 ML DBP/Ag(110) film produced at RT and annealed to increasing T (Figure 2). The Br 3d spectrum (Figure 2a, bottom trace) consists of two components with the Br $3d_{5/2}$ peak centered at E_b=70.2 and 68.1 eV, respectively. The former is ascribed to Br–C bonds in the DBP molecules while the latter corresponds to Br atoms chemisorbed on the silver substrate.[13, 33, 42] The C 1s spectrum obtained after the deposition at RT (Figure 2b) shows two

distinct features. The weak but clearly visible component at E_b= 283.1 eV is a typical fingerprint of C–Ag bonds, that are formed when metal adatoms from the substrate react with the C radical created after C–Br bond dissociation.[31, 33, 34] The second feature is the broad peak centered at 284.3 eV, which corresponds to aromatic carbon atoms in the pyrene units. Its shape can be modeled by the superposition of two components at E_b= 284.1 and 284.4 eV, assigned to C atoms bound to other C atoms only (C–C component) or to both H and C atoms (C–H component), respectively.[33, 43-45] At RT, the intensity of the Br 3d component at E_b=70.2 eV implies a relatively high fraction of intact or partially debrominated DBP molecules. They can be identified mainly with the DBP units in the second layer, which do no interact with the catalytic substrate and thus do not break the Br-C bonds. Although most of the second layer DBP molecules desorb after mild annealing to 100 °C (see Temperature Programmed XPS in ESI), in the experiment of Figure 2a a small amount of undissociated Br–C bonds is detected even after heating up to 200 °C. Such behavior is in contrast with the one observed starting from a DBP coverage Θ<1 ML, for which complete debromination occurs at 100 °C (not shown). Therefore, apart from the contact with the substrate, also other effects must play a role in the Br–C bond activation. We propose that, at the lower temperature, the DBP crowdedness at saturation coverage reduces the dissociation probability, reasonably inhibiting the adsorption configurations most favorable for the on-surface dissociation and/or limiting the availability of the active sites.

The C/Br atomic concentration ratio, determined form the photoemission intensities, is (8.7 ± 0.9) after deposition at RT. Such value is well compatible with the expected stoichiometry ratio of 8 and indicates a negligible recombination and desorption of Br_2 molecules or other Br compounds upon dissociation at RT. However, after annealing to 150 °C, the Br 3d intensity drops more than the C 1s one (see Figure 2c), so the C/Br ratio increases to (11.3 ± 1.3). This suggests that a small fraction of Br atoms desorbs during the annealing to 150 °C, while the DBP radicals or biradicals remain on the substrate.

In view of these considerations and going back to the high resolution STM images of Figure 1, we observe that in both structures I and II there are two small, round protrusions for each DPB unit (yellow and green arrows). For the disordered structure III, on the contrary, a quantification is more difficult. Comparing these images with the XPS results, we find that the density of bright protrusions in structures I and II slightly exceeds the expected population of Br atoms at 150 °C. A possible explanation is that some early desorption of Br can be induced by spurious effects in the more disordered areas; alternatively, one of the two bright features in either structure I or II must correspond to an Ag atom bound to the pyrene groups to form organometallic proto-polymers. This second hypothesis is supported by the presence of a small but

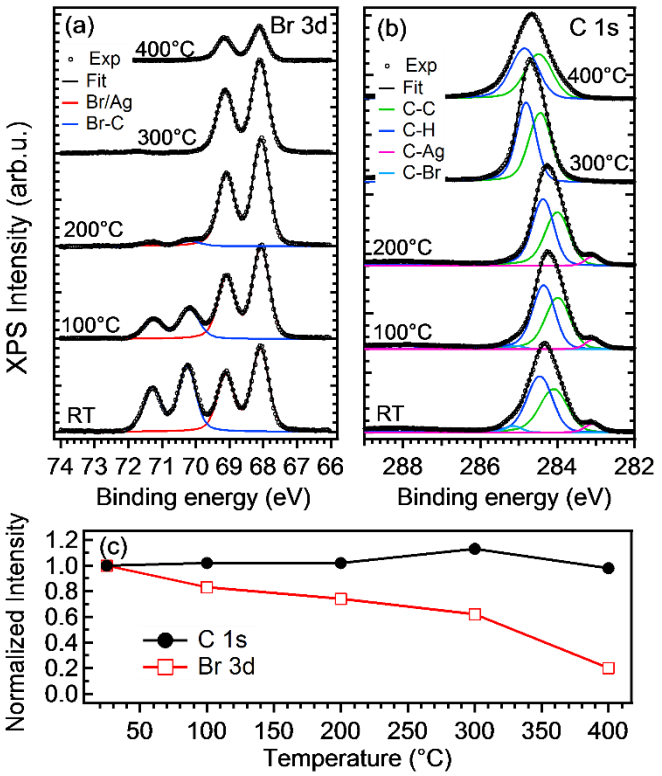

Figure 2. *(a) Br 3d and (b) C 1s core level spectra of 1.2 ML DBP deposited on the Ag(110) substrate kept at RT and after annealing at the indicated temperatures. (c) Total intensity of the Br 3d and C 1s spectra as a function of the annealing temperature, normalized to the initial values after the deposition.*

significant C–Ag intensity in the C 1s region, which remains stable up to 200 °C. Similar organometallic structures have been widely reported also for other halogenated aromatic hydrocarbons.[16, 28, 33-35, 42, 46, 47] The simulated STM image (see Figure S5 in the ESI) of a fully debrominated DBP monomer in presence of Br and Ag adatoms shows a molecular skeleton formed by four bright lobes, corresponding to the benzene rings, and very similar roundish bright spots for Ag and Br adatoms. It confirms, therefore, the difficulty of identifying the chemical nature of the bright protrusions observed experimentally.

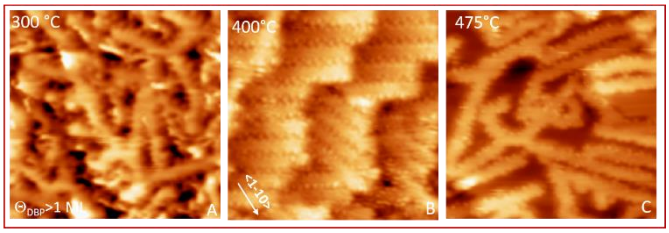

Figure 3. *STM images of the DBP multilayer produced at RT and annealed to increasing T. A) 300 °C, corresponding to the initial stage of the polymerization process. B) 400 °C; well-defined domains of parallel polymers fully cover the surface. C) 475 °C; formation of a polymer network. In all cases, image size: 12.5 x 12.5 nm². V=0.15 V in A) and -0.05 V in B) and C). Since negligible bias dependence was observed in the range -0.25 V <V<+0.50 V (see Figure S3 in the SI), direct comparison of the images is allowed.*

The first signs of C–C coupling and covalent polymerization of the organometallic chains are observed after annealing to 300

°C. The STM images (see Figure 3A) show the presence of short conjugated polymers with corrugated edges and arranged in a disordered way on the surface. This structural transformation is accompanied by changes in the chemical form of the overlayer and adsorbate–substrate interaction, as determined by XPS. In the C 1s region (Figure 2b), the C–Ag component at E_b=283.1 eV disappears and the whole spectrum is shifted by about 0.4 eV towards higher binding energies. The C 1s shift is dominated by the energy level alignment at the adsorbate/metal interface, as evidenced by temperature programmed XPS and work function measurements (see ESI for details). TPR experiments, performed to gain a complementary information about the sequence of thermally activated surface reactions of DBP, show that the dehydrogenation process takes place simultaneously (see Figure 4). Although the signals of several possible desorption products were monitored, we observed significant intensity only in the case of hydrogen and hydrobromic acid. At about 280 °C both H_2 and HBr molecules start to desorb from the surface, producing a maximum at about 380 °C, then the signals decrease. These data clearly suggest that the Br atoms are quite stable on the Ag(110) until some hydrogen coming from thermally activated cyclodehydrogenation is produced. Thanks to this local source of H atoms, HBr can be produced, which is immediately desorbed from the surface. A similar behaviour was also observed in the case of the Br removal on the Au(111) surface during the formation of nanoribbons starting from DBBA molecules.[48]

Increasing the annealing temperature to 400 °C (Figure 3B) causes a significant ordering of the nanostructures. The surface is now covered by domains of straight graphene nanoribbons with preferential orientation -30° and -55° off the <1-10> direction and length (up to ~10 nm, on average) limited apparently only by the width of the Ag(110) terraces. The process is accompanied by a significant desorption of the Br adatoms, as indicated by the reduction of the Br 3d signal in the XPS spectrum (Figure 2ac). If the sample is brought to 475 °C (Figure 3C), the total coverage reduces, desorption of Br adatoms becomes complete and further de-hydrogenation of the polymers occurs. Indeed STM images show that the chains become longer, merge together in a network arranged randomly on the surface and leave bare Ag areas exposed, while XPS (Figure2c and Figure S1 of ESI) and TPR measurements (Figure 4) provide the chemical information.

It is evident that the optimal temperature for the surface-catalyzed synthesis of ordered arrays of GNRs starting from the DBP molecules is about 400 °C. We therefore concentrate on the preparations at this temperature for further analysis.
In Figure 5, we show how the final arrangement of the covalent network depends on the initial DBP coverage and on the annealing treatment. Panels A and B compare the patterns of conjugated polymers obtained starting from a DBP sub-monolayer and a DBP multilayer, respectively, and annealing them to 150 °C for 2 minutes and then to 400 °C for 1 minute.

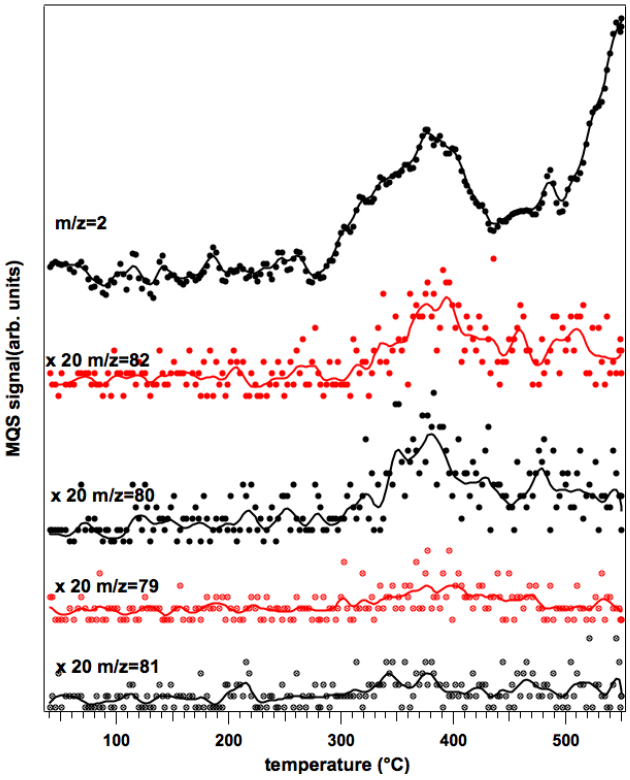

Figure 4. *TPR spectra of the Ag(110) surface covered by 1 ML of DBP and annealed with a constant thermal gradient of 2.5 °C/s up to 550 °C. The traces correspond to the QMS signal coming form the most probable desorption products: H^+_2(m/z=2), Br^+ (m/z=79, 81), HBr^+ (m/z=80, 82). The increase of the m/z=2 signal above 450 °C is an artefact due to desorption from the filament and from the sample holder. The absence of peaks for T<100 °C, i.e. in correspondence of the desorption of the multilayer, is explained by the combination of two factors: the slightly lower initial coverage of this experiment with respect to the XPS and STM ones and the very low cracking probability of non-dissociated DBP molecules at the masses investigated here.*

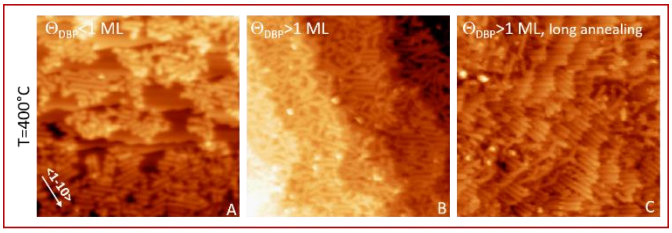

Figure 5. *STM images of the Ag(110) surface covered by GNRs obtained with different protocols: A) Annealing a DBP submonolayer produced at RT to 150 °C for 2 minutes and then to 400 ° C for 1 minute (V=0.15 V). B) Same as A), starting from a multilayer of DBP (V=-0.35 V). C) Annealing a DBP multilayer to 150 °C for 15 minutes and then to 400 ° for 3 minutes (V=-0.05 V). In all cases, image size: 40.5x40.5 nm².*

As evident from the inspection of the STM images, polymerization and formation of graphene-like nano-ribbons occur in both cases, but the initial coverage is relevant in determining the length and order of the structures. As expected, in the first case (panel A) the ribbons do not cover

the whole Ag surface. Less obviously, they are short and forming very small domains, with a poor directionality. Since at 150 °C the surface is covered by large islands of organometallic compounds alternated to bare Ag regions (not reported), such behavior is indicative of significant desorption and of a limited mobility of the DBP radicals already organized in a self-assembled structure. Taking the bare Ag(110) surface as a reference, for this preparation it is possible to measure the apparent height of the ribbons, which is (1.0 ± 0.2) Å, with a negligible bias dependence for -1.3 V < V < +1.3 V. When starting from Θ>1 ML (panel B), the length of the nanoribbons increases and only small areas of bare Ag are visible in correspondence to the conjunction of ribbons with different orientation. The supra-molecular arrangement is however still quite disordered. To improve it, a freshly prepared DBP multilayer was kept at 150 °C for 15 minutes and subsequently heated to 400 °C for 3 minutes. The result of this procedure is reported in panel C, showing extended areas in which the conjugated polymers arrange parallel to each other in a compact geometry. The prolonged annealing at intermediate temperature has therefore favored the organization of the precursor organometallic chains in large domains and, possibly, selected a preferential geometry between patterns I and II of Figure 1. Therefore this one appears to be an optimal protocol for the growth of extended domains of parallel conjugated polymers.

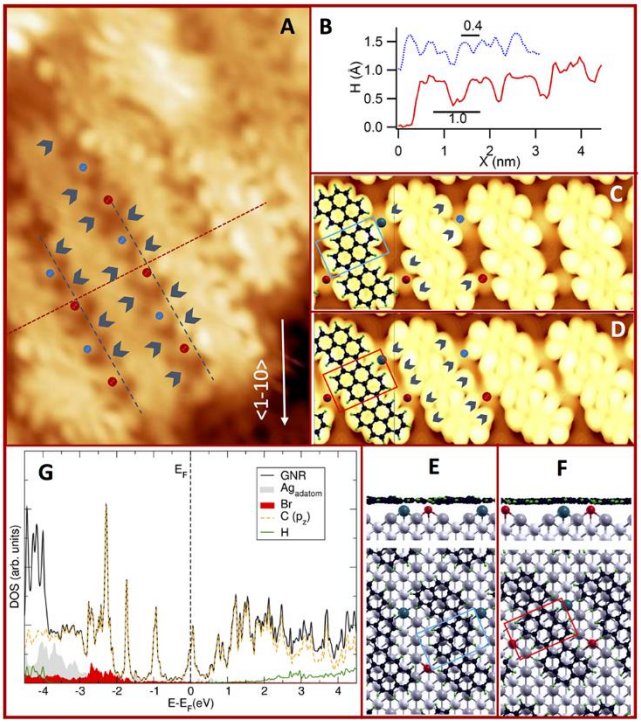

Figure 6. *A) High resolution STM image of the GNRs (image size: 4.0 x5.8 nm², V=-0.05 V). The presence of an internal structure is evident and is confirmed by the line profile cut along the red dashed line reported in panel B (red trace). The blue and red dots indicate the protrusions in-between the GNRs, tentatively assigned to Ag and Br adatoms for comparison with the simulated images of panels C and D. The small grey arrows indicate, on the contrary, protrusions which are part of the GNR. The overall periodicity along the channel is evidenced by the profile marked by the blue dashed lines and reported in panel B (blue trace). C) Calculated STM images with and without balls-and-sticks model superposition for the trimer with alternating chirality. D) Same as C) for the homochiral trimer. E-F) Corresponding optimized structure for the DBP trimers of panels C and D, respectively, with Ag (blue) and Br (red) adatoms in hollow position. Blue and red rectangles highlight the central molecular unit, which has different chirality in the trimers. G) Calculated PDOS for the structure in E). The experimental STM image has been rotated to be coherent with the directions used in the simulation.*

Figure 6A shows a high resolution image of GNRs produced by the "prolonged annealing" protocol of Figure 5C. As already mentioned, they form a compact pattern of polymers arranged parallel on the surface and oriented -30° off <1-10>. They have quite corrugated edges and an evident internal structure. The latter is apparent also from the height profile plotted in panel B (red curve), since the part running across the body of the GNRs is not flat but clearly modulated by the different local electron density. The same line scan allows to determine the periodicity of the structure (~10 Å) in the direction across the ribbons. The presence of small round protrusions in between the ribbons (marked by red and blue dots) is evident in panel A. Although they present a rather regular pattern in this image, they are not always evenly distributed over the surface, indicating that they are not part of the GNR itself but, most probably, residual Ag or Br adatoms (a 20% of the initial Br coverage is still adsorbed, according to XPS spectra – see Figure 2a). In the image of Figure 6A, they are regularly spaced at a distance of (7.5±0.5) Å from each other. This periodicity combines with the one generated by the protruding edges of the GNRs (marked as grey arrows) to give an overall periodicity of ~4 Å measured along the channels in between the GNRs (blue profile in panel B).

The internal structure and the edge geometry of the experimentally observed nanostructure could not be fully resolved by STM images only. To clarify these details, we performed DFT geometry optimization of two different debrominated and C–C conjugated DBP trimers on a 3×7 supercell Ag(110) surface model (see Figure 6E and F) and we simulated the corresponding STM images (Figure 6C and D, respectively). The two structures differ by the configuration of the central DBP unit (compare blue and red rectangles in Figure 6E and F). The one in panel E models an achiral ribbon since it is made by flipping the central unit with respect to the lateral ones, thus giving an alternated assembly of the two metal-DBP enantiomers along the trimer. The trimer in panel F, on the contrary, is formed by assembling the same metal-DBP enantiomers and holds then for the case in which chiral recognition is active.

We first consider the polymer with alternating chirality of Figure 6E. The barycenters of the repeated polymer result to be at a distance of about 11.4 Å, i.e. reasonably close to the experimentally measured value. The minimum distance between H atoms is ~ 3.6 Å. Additionally, one Ag and one Br adatom were introduced in the hollow positions in between the trimers. For Ag adatoms the hollow site is by far (0.3 eV) the most stable one, whereas for Br adatoms the bridge and

hollow positions are almost equivalent (with a -0.03 eV difference in energy).

When the nanoribbons are formed on the clean Ag(110) surface, they physisorb at an equilibrium distance from the substrate of ~2.8 Å with an adhesion energy (ΔE_{adh}) of about -1.1 eV per DBP unit. The energy gain associated with the formation of two C–C bonds, in a DBP dimer or trimer, has been estimated to be about 1 eV in gas-phase (see Figure S7 in SI). The consequent release of two HBr molecules is favored (by -0.97 eV) compared to the formation of H_2 and Br_2. After debromination and dehydrogenation of DBP molecules, the formation of ribbons takes place and weak dispersion forces bind the ribbons to the substrate, with only a small electron charge donation from the silver substrate to the ribbons (see Figure S8 in the ESI). Figure 6G reports the projected density of states (PDOS) for the ribbon of alternate chirality adsorbed on the Ag(110) surface (as represented in Figure 6E), showing that close to the Fermi level the ribbon presents only π states. The orientation of the ribbons with respect to the Ag substrate has a negligible influence on the adhesion energy (with only a difference of 0.03 eV per DBP unit for a -30º or -55º rotation with respect to the 110 rows), confirming the weak interactions between the DBP and the support.

The homochiral ribbon (Figure 6F) behaves similarly to the one with alternating chirality and it is almost iso-energetic. Therefore it is not possible to determine the internal structure and the edge geometry of the experimentally observed GNRs based on geometry optimization only. Comparison with the simulated STM images of Figure 6C and D is indeed essential in this respect. On one hand it is evident that in both the investigated configurations the DBP-derived GNRs present a (2,1) sequence of zig-zag and armchair edge sites, with a high edge corrugation. On the other hand, the simulated configuration with alternate chirality results in much better agreement with the measured counterparts (compare Figure 6A and Figure 6C): couples of bright lobes along the edges (highlighted by grey arrows) alternate to less protruding lobes, corresponding to the flipped unit and not present for the homochiral ribbon.

Simulations at different bias voltage (see Figure S9 in ESI) show negligible changes in the STM contrast, in agreement with the experimental findings (see Figure S3 in ESI). We note, however, that the appearance of Ag or Br adatoms between the ribbons is quite similar in the simulated images, so that it is not possible at this stage to make a conclusive assignment of the additional protrusions observed in the experimental image to either one or the other species. The calculated PDOS shows the presence of Ag and Br states for $(E-E_F)<-2$ eV, but this energy region was not tested experimentally due to the strong tip-surface interactions. Moreover, a simulation performed without Ag and Br adatoms (see Figure S10 in SI) yields very similar results for both the adsorption structure and STM contrast of the ribbons, yet with a clear lack of bright spots between them. This is coherent with the extended formation of GNRs in spite of the irregular presence of the additional adatoms, which have a significantly smaller coverage.

Statistical analysis over a few hundred GNRs (see table T1 in ESI) indicates that they are monodispersed in width. The average value of (9.9±0.6) Å is the same, within experimental error, for both orientations of the well-ordered ribbons (Figure 5C) and it is compatible with the corresponding quantity measured for the disordered nanostructures of Figure 5AB. Furthermore, taken into account the convolution with the STM tip, the experimentally measured width is compatible with the dimension of a single pyrene unit. This suggests that each GNR is formed by a single row of molecules polymerized together to form unidimensional chains. The latter are significantly narrower than those formed from the more common DBBA precursor.[18, 20] Since this parameter is fundamental in determining the electronical properties of the nano-ribbon, the ability to grow a monodispersed array of nanostructures represents a significant achievement in the field. In addition, according to the model proposed in Figure 6E, the GNRs present a sequence of zig-zag and armchair edge sites in a (2,1) sequence. This configuration is rather peculiar, since in most cases only one kind of site is available.[18, 32] Furthermore, GNRs with special edge-site sequences may present particular electronic properties in view of the localized electronic states at the zig-zag edges predicted for free-standing GNRs[5] and observed experimentally for nanostructures much larger than those of the present work[49].

Besides DBBA[18, 19, 21, 22, 50], only a few molecules have been tested as precursors for the surface-assisted growth of unidimensional graphene-like structures on coinage metal surfaces[32, 35], even less on silver[33]. It is remarkable that only in rare cases the final result could be attained, which indicates a specificity of the substrate but, first of all, of the molecule. Surface polymerization of DBP undergoes a reaction path quite different from DBBA. In the latter case the Ullman reaction takes advantage of an easy rotation of the two anthryl sub-molecular units around the C–C bond connecting them; therefore, the molecules do not lay flat on the surface. The freedom connected to the torsional angle is fundamental to prevent the steric hindrance between hydrogen atoms during the C–C bond formation. The DBP molecules, on the other hand, are rigidly planar and the problem of the steric hindrance of the hydrogen atoms is solved by positioning the Br atoms on peripheral positions of the molecular back bone. Comparison with the 5,11-dibromotetracene (DBT) on Ag(110)[33] is paradigmatic to evidence the role of molecular geometry. Although both molecules consist of four benzene rings, DBT has a rod-like shape. After debromination, the radical is aligned along the <1-10> direction and anchored in such orientation by C–Ag bonds. The radical C atom is sided by C–H groups along the zig-zag edge; in addition, substrate-directed adsorption suppresses dehydrogenative coupling at mild temperatures. DBP, on the contrary, is a more compact and planar molecule. It has shorter zig-zag edges with respect

to DBT, so that the radical formed by the dehalogenation is inserted in a more open geometry, where the C–H bonds of the neighboring C atoms (C_α) are not parallel, but 60° off. This prevents the repulsion between C–H groups of neighboring radicals and allows the formation of the C–C bonds, which was impeded in the case of DBT. The apparently weaker radical–surface interaction, probably combined with a more favorable molecular geometry, enhances the overall mobility of the monomer units and favors molecular network rearrangement by rotation, hence the formation of elongated polymers by C–C coupling. Therefore, our results suggest that also fully condensed aromatic molecules with a rigid backbone can enter the arena of surface catalysed polymerizations and lead to the formation of quite special nanoribbons.

The behavior of an as-deposited DBP monomer, as well as the debromination steps, have been simulated on the Ag(110) surface (see Figure S4 in the SI), showing that the binding energies are about 0.4 eV weaker than for DBT [33]. Such observation underlines the peculiar role of DBP as a precursor for the formation of GNRs. A hint about the possible mechanism leading to the formation of such regular patterns of GNRs is suggested by TPR data, in particular by the information about the Br desorption temperature. The Br atoms are very stable and strongly adsorbed on the Ag surface until T>280 °C. When adsorbed, they may act as spacers between the metallorganic protopolymers, so that the cyclodehydrogenation process takes place in a geometrically controlled environment, leading to a very well-ordered surface morphology. Only when the cyclodehydrogenation reaction has released enough hydrogen on the surface, the transient template constituted by the Br atoms is removed as HBr. This ability of Br to direct the self-assembly of carbon nanostructures has been recently demonstrated also in the case of the reaction of DBBA on different copper surfaces.[22]

All these considerations reinforce the importance of the nature of the precursor molecules in the surface-assisted growth of C-based nanostructures and allow to foresee the possibility, in the near future, to produce GNRs with tailored electrical and geometric properties by using suitably engineered precursor molecules.

Finally, we mention that the sequence of zig-zag and armchair edges produces, locally, a (2,1) chiral configuration. This is true both for the polymerization of DBP radicals in racemic (Figure 6E) or homochiral (Figure 6F) sequence. As mentioned, the two different configurations were calculated to determine if chiral recognition is energetically favored, but very close values of the adsorption energies were found. On the other hand, the comparison of high resolution images with the result of simulated STM maps suggests that the flipped configuration presents the best agreement with the experiment. We conclude that chiral recognition is not determining in the formation of GNRs. This is coherent with the predominant extension of the racemic structure I at 150°C.

Some irregularities of the edges are however present in the GNRs pattern and we suggest that they correspond to a fault in the alternate sequence of D- and L- molecules forming the polymer. Therefore, the formation of GNRs with a random sequence of D- and L-type DBP units, and hence also the formation of locally homochiral sequences, may occasionally occur. This is not surprising, also in view of the very similar energy calculated for the homochiral and flipped trimers of Figure 6.

4. Conclusions

In conclusion, we have reported on the formation of achiral graphene nanoribbons with local (2,1) zig-zag and armchair edges on Ag(110) by surface assisted polymerization of (1,6)-dibromopyrene precursors. These nanostructures, monodispersed in width, organize in ordered patterns of parallel ribbons or, at higher T, in extended polymer networks. Due to the conformation of the precursor molecule, the GNRs show edges with zig-zag and armchair sites alternated in sequence. Besides the interest of the result in itself for the foreseen applications of graphene-like 1D structures in fields such as nanoelectronics, we confirm here the importance of the initial choice of the precursor for the synthesis of selected nano-structures. Furthermore, we demonstrate the valuable use of condensed aromatic molecules with a rigid backbone, and of pyrene derivatives in particular, as candidates for surface catalysed polymerization leading to the formation of quite special nanoribbons.
In the near future we foresee the possibility to tune the geometrical and electronic properties of GNRs fabricated with a bottom-up approach by on-purpose design of suitable precursors, as it is already happening for other classes of molecules.

Acknowledgements

This work was founded by MIUR through project FIRB Futuro in Ricerca 2012 N. RBFR128BEC and progetto premiale ABNANOTECH.

Notes and references

1. M. Batzill, *Surface Science Reports*, 2012, **67**, 83–115.
2. Y. Zhu, S. Murali, W. Cai, X. Li and J. W. Suk, *Advanced Materials*, 2010, **22**, 3906–3924.
3. X. Wang, Y. Ouyang, X. Li, H. Wang, J. Guo and H. Dai, *Physical Review Letters*, 2008, **100**, 206803.
4. X. Li, X. Wang, L. Zhang, S. Lee and H. Dai, *Science*, 2008, **319**, 1229-1232.
5. K. Nakada, M. Fujita, G. Dresselhaus and M. S. Dresselhaus, *Physical Review B*, 1996, **54**, 17954-17961.

6. Y. C. Chen, D. G. de Oteyza, Z. Pedramrazi, C. Chen, F. R. Fischer and M. F. Crommie, *ACS Nano*, 2013, **7**, 6123–6128.
7. J. Baringhaus, M. Ruan, F. Edler, A. Tejeda, M. Sicot, A. Taleb-Ibrahimi, A.-P. Li, Z. Jiang, E. H. Conrad, C. Berger, C. Tegenkamp and W. A. de Heer, *Nature*, 2014, **506**, 349-354.
8. I. Palacio and e. al., *Nano Letters*, 2014, **15**, 182-189.
9. X. Yang, X. Dou, A. Rouhanipour, L. Zhi, H. J. Raeder and K. Muellen, *Journal of the American Chemical Society*, 2008, **130**, 4216-4217.
10. M. Y. Han, B. Oezyilmaz, Y. Zhang and P. Kim, *Physical Review Letters*, 2007, **98**, 206805.
11. L. Jiao, L. Zhang, X. Wang, G. Diankov and H. Dai, *Nature*, 2009, **458**, 877-880.
12. D. V. Kosynkin, A. L. Higginbotham, A. Sinitskii, J. R. Lomeda, A. Dimiev, B. K. Price and J. M. Tour, *Nature*, 2009, **458**, 872-U875.
13. J. Eichhorn, T. Strunskus, A. Rastgoo-Lahrood, D. Samanta, M. Schmittel and M. Lackinger, *Chemical Communications*, 2014, **50**, 7680-7682.
14. S. W. Hla, L. Bartels, G. Meyer and K. H. Rieder, *Physical review letters*, 2000, **85**, 2777-2780.
15. L. Lafferentz, F. Ample, H. Yu, S. Hecht and C. Joachim, *Science*, 2009, **323**, 1193-1197.
16. Q. Fan, J. M. Gottfried and J. Zhu, *Accounts of Chemical Research*, 2015, **48**, 2484-2494.
17. G. Franc and A. Gourdon, *Physical Chemistry Chemical Physics*, 2011, **13**, 14283-14292.
18. J. Cai, P. Ruffieux, R. Jaafar, M. Bieri, T. Braun, S. Blankenburg, M. Muoth, A. P. Seitsonen, M. Saleh, X. Feng, K. Müllen and R. Fasel, *Nature*, 2010, **466**, 470-473.
19. K. A. Simonov, N. A. Vinogradov, A. S. Vinogradov, A. V. Generalov, E. M. Zagrebina, N. Martensson, A. A. Cafolla, T. Carpy, J. P. Cunniffe and A. B. Preobrajenski, *Journal of Physical Chemistry C*, 2014, **118**, 12532-12540.
20. P. Ruffieux, J. Cai, N. C. Plumb, L. Patthey, D. Prezzi, A. Ferretti, E. Molinari, X. Feng, K. llen and C. A. Pignedoli, *Acs Nano*, 2012, **6**, 6930-6935.
21. S. Linden, D. Zhong, A. Timmer, N. Aghdassi, J. H. Franke, H. Zhang, X. Feng, K. Müllen, H. Fuchs and L. Chi, *Physical review letters*, 2012, **108**, 216801.
22. K. A. Simonov, N. A. Vinogradov, A. S. Vinogradov, A. V. Generalov, E. M. Zagrebina, G. I. Svirskiy, A. A. Cafolla, T. Carpy, J. P. Cunniffe, T. Taketsugu, A. Lyalin, N. Mårtensson and A. B. Preobrajenski, *ACS Nano*, 2015, **9**, 8997-9011.
23. Y. Li, W. Zhang, M. Morgenstern and R. Mazzarello, *Physical Review Letters*, 2013, **110**, 216804.
24. J. Liu, B.-W. Li, Y.-Z. Tan, A. Giannakopoulos, C. Sanchez-Sanchez, D. Beljonne, P. Ruffieux, R. Fasel, X. Feng and K. Müllen, *Journal of the American Chemical Society*, 2015, **137**, 6097-6103.
25. P. Han, K. Akagi, F. Canova, H. Mutoh, S. Shiraki, K. Iwaya, P. S. Weiss, N. Asao and T. Hitosugi, *ACS nano*, 2014, **8**, 9181-9187.
26. P. Han, K. Akagi, F. F. Canova, R. Shimizu, H. Oguchi, S. Shiraki, P. S. Weiss, N. Asao and T. Hitosugi, *ACS Nano* 2015, **12**, 12035– 12044.
27. C. Sánchez-Sánchez, T. Dienel, O. Deniz, P. Ruffieux, R. Berger, X. Feng, K. Müllen and R. Fasel, *ACS Nano*, 2016, **10**, 8006-8011.
28. C. Zhang, Q. Sun, H. Chen, Q. Tan and W. Xu, *Chemical Communications*, 2014, **51**, 495-498.
29. Q. Fan, C. Wang, Y. Han, J. Zhu, J. Kuttner, G. Hilt and M. J. Gottfried, *ACS nano*, 2013, **8**, 709-718.
30. M. Chen, J. Xiao, H.-P. Steinrück, S. Wang, W. Wang, N. Lin, W. Hieringer and M. J. Gottfried, *The Journal of Physical Chemistry C*, 2014, **118**, 6820-6830.
31. A. Basagni, F. Sedona, C. A. Pignedoli, M. Cattelan, L. Nicolas, M. Casarin and M. Sambi, *J. Am. Chem. Soc.* , 2015, **137**, 1802-1808.
32. A. Kimouche, M. M. Ervasti, R. Drost, S. Halonen, A. Harju, P. M. Joensuu, J. Sainio and P. Liljeroth, *Nature Communications*, 2015, **6**, 10177.
33. I. Píš, L. Ferrighi, T. Nguyen, S. Nappini, L. Vaghi, A. Basagni, E. Magnano, A. Papagni, F. Sedona, C. Valentin, S. Agnoli and F. Bondino, *The Journal of Physical Chemistry C*, 2016, **120**, 4909-4918.
34. L. Ferrighi, I. Píš, T. Nguyen, M. Cattelan, S. Nappini, A. Basagni, M. Parravicini, A. Papagni, F. Sedona, E. Magnano, F. Bondino, C. Valentin and S. Agnoli, *Chemistry (Weinheim an der Bergstrasse, Germany)*, 2015, **21**, 5826-5835.
35. A. Basagni, L. Ferrighi, M. Cattelan, L. Nicolas, K. Handrup, L. Vaghi, A. Papagni, F. Sedona, C. Valentin, S. Agnoli and M. Sambi, *Chemical Communications*, 2015, **51**, 12593-12596.
36. B. Kim, Y. Park, J. Lee, D. Yokoyama, J.-H. Lee, J. Kido and J. Park, *Journal of Materials Chemistry C*, 2013, **1**, 432-440.
37. I. Horcas, R. Fernandez, J. M. Gomez-Rodriguez, J. Colchero, J. Gomez-Herrero and A. M. Baro, *Review of Scientific Instruments*, 2007, **78**, 013705.
38. I. Hamada and M. Otani, *Physical Review B*, 2010, 153412.
39. P. Giannozzi, S. Baroni and N. Bonini, *Journal of Physics: Con. Matter*, 2009, **21**, 395502.
40. J. Tersoff and D. R. Hamann, *Scanning Tunneling Microscopy*, 1985.
41. Q. Chen, D. J. Frankel and N. V. Richardson, *Surface Science*, 2002, **497**, 37-46.
42. R. Gutzler, L. Cardenas, J. Lipton-Duffin, M. Garah, L. E. Dinca, C. E. Szakacs, C. Fu, M. Gallagher, M. Vondráček, M. Rybachuk, D. F. Perepichka and F. Rosei, *Nanoscale*, 2014, **6**, 2660-2668.
43. R. Kakavandi, S.-A. Savu, A. Caneschi, T. Chassé and M. Casu, *Chemical Communications*, 2013, **49**, 10103-10105.
44. S. A. Savu, I. Biswas, L. Sorace, M. Mannini, D. Rovai, A. Caneschi, T. ChassØ and M. B. Casu, *Chemistry A European Journal*, 2013, **19**, 3445-3450.
45. A. Schöll, Y. Zou, M. Jung, T. Schmidt and R. Fink, *The Journal of Chemical Physics*, 2004, **121**, 10260.
46. J. Park, K. Kim, K.-H. Chung, J. Yoon, H. Kim, S. Han and S.-J. Kahng, *The Journal of Physical Chemistry C*, 2011, **115**, 14834-14838.
47. K. H. Chung, B. G. Koo, H. Kim, J. K. Yoon and J. H. Kim, *Phys.Chem. Chem. Phys.*, 2012, **14**, 7304–7308.
48. C. Bronner, J. Björk and P. Tegeder, *The Journal of Physical Chemistry C*, 2014, **119**, 486-493.
49. C. Tao, L. Jiao, O. V. Yazyev, Y.-C. Chen, J. Feng, X. Zhang, R. B. Capaz, J. M. Tour, A. Zettl, S. G. Louie, H. Dai and M. F. Crommie, *Nature Physics*, 2011, **7**, 616-620.
50. L. Massimi, O. Ourdjini, L. Lafferentz, M. Koch, L. Grill, E. Cavaliere, L. Gavioli, C. Cardoso, D. Prezzi, E. Molinari, A. Ferretti, C. Mariani and M. Betti, *The Journal of Physical Chemistry C*, 2015, **119**, 2427-2437.